Afferent modulation of neonatal rat respiratory rhythm *in vitro*: cellular and synaptic mechanisms

Nicholas M. Mellen, Maryam Roham and Jack L. Feldman

Systems Neurobiology Laboratory, Department of Neurobiology, David Geffen School of Medicine at the University of California Los Angeles, Los Angeles, CA 90095-1763, USA

In mammals, expiration is lengthened by mid-expiratory lung inflation (Breuer-Hering Expiratory reflex; BHE). The central pathway mediating the BHE is paucisynaptic, converging on neurones in the rostral ventrolateral medulla. An *in vitro* neonatal rat brainstem–lung preparation in which mid-expiratory inflation lengthens expiration was used to study afferent modulation of respiratory neurone activity. Recordings were made from respiratory neurones in or near the pre-Bötzinger Complex (preBötC). Respiratory neurone membrane properties and BHE-induced changes in activity were characterized. Our findings suggest the following mechanisms for the BHE: (i) lung afferent signals strongly excite biphasic neurones that convey these signals to respiratory neurones in ventrolateral medulla; (ii) expiratory lengthening is mediated by inhibition of rhythmogenic and (pre)motoneuronal networks; and (iii) pre-inspiratory (Pre-I) neurones, some of which project to abdominal expiratory motoneurones, are excited during the BHE. These findings are qualitatively similar to studies of the BHE *in vivo*. Where there are differences, they can largely be accounted for by developmental changes and experimental conditions.

(Resubmitted 6 January 2004; accepted after revision 4 February 2004; first published online 6 February 2004)
Corresponding author N. M. Mellen: Systems Neurobiology Laboratory, Department of Neurobiology, David Geffen School of Medicine at the University of California Los Angeles, Los Angeles, CA 90095-1763, USA.
Email: nmellen@ucla.edu

In behaving mammals, respiration is continuously modulated as a function of metabolic demand, state of arousal, posture, temperature, etc. Signals related to these variables, conveyed by descending and sensory afferents, converge on respiratory rhythm-generating networks in the ventrolateral medulla. Respiratory afferent modulation has been studied extensively in humans (q.v., Widdicombe & Lee, 2001) and, more invasively, in a variety of juvenile or adult mammalian preparations (von Euler, 1983; Lindsey *et al.* 1987, 2000; Schwarzacher *et al.* 1995; Gray *et al.* 2001, Mitchell & Johnson, 2003; Dutschmann & Paton, 2003). A limitation of these *in vivo* studies is that the respiratory networks are relatively inaccessible, and basic rhythmogenic mechanisms remain poorly understood. To overcome these limitations, neonatal rodent *in vitro* preparations that produce respiratory-related rhythm unmodulated by sensory feedback have been developed (Smith & Feldman, 1987; Onimaru & Homma, 1987; Smith *et al.* 1991) and extensively used to investigate essential rhythmogenic mechanisms (Smith *et al.* 1993; Rekling & Feldman, 1998).

A basic problem impeding our understanding of respiratory rhythm generation and modulation is that while mappings between *in vitro* and *in vivo* data have been proposed (Feldman *et al.* 1990; Richter & Spyer, 2001), they are difficult to test experimentally: differences due to experimental conditions and development interact and it is difficult to control for them. Here we reincorporate lung afferent feedback *in vitro* so as to be able to compare cellular and systems level responses *in vitro* to similar studies carried out *in vivo* (Hayashi *et al.* 1996), and to assess whether afferent perturbations to respiratory rhythm can be used to differentiate between rhythmogenic and sensory relay networks.

We use an *in vitro* neonate rat brainstem–spinal cord preparation in which the lungs and their vagal innervation are retained (Murakoshi & Otsuka, 1985; Mellen & Feldman, 1997). In this preparation, lung inflation at pressures in the physiological range (2–5 mmH_2O; Widdicombe, 1961) modulates respiratory rhythm. Transient lung inflation during inspiration shortens inspiration (Mellen & Feldman, 2000, 2001) and sustained

 DOI: 10.1113/jphysiol.2004.060673

mid-expiratory lung inflation lengthens expiration (Mellen & Feldman, 1997). These responses match those seen in mammals (Breuer, 1868) and are referred to as the Breuer-Hering inspiratory reflex (BHI) and Breuer-Hering expiratory reflex (BHE), respectively (von Euler, 1983, Feldman, 1986).

The Breuer-Hering reflexes are elicited by activation of slowly adapting pulmonary receptors (SARs; Adrian, 1933, Schelegle & Green, 2001). These provide glutamatergic input (Bonham *et al.* 1993) to second-order neurones in nucleus tractus solitarii (NTS). These second order neurones project to the ventrolateral medulla, as far rostral as the caudal margin of the facial nucleus (Ezure & Tanaka, 1996; Ezure *et al.* 2002) and also inhibit rapidly adapting relay neurones in the caudal NTS (Ezure & Tanaka, 2000).

In adult cats, electrical stimulation of the vagus nerve produces short latency EPSPs in late inspiratory (Late-I; Feldman & Cohen, 1978; Cohen *et al.* 1993) and decrementing expiratory (E-Dec; Feldman & Cohen 1978) neurones, demonstrating vagal-mediated excitatory drive to expiratory neurones in the ventrolateral medulla. E-Dec neurones, in turn, inhibit a broad range of inspiratory neurones (Lindsey *et al.* 1987; Segers *et al.* 1987). Similar observations were made in rats (Ezure & Manabe, 1988; Manabe & Ezure, 1988; Parkes *et al.* 1994). Thus, electrical stimulation of the vagus nerve reliably elicits IPSPs in inspiratory neurones and lung inflation reduces respiratory-related phasic depolarization in all inspiratory neurones (Hayashi *et al.* 1996). These results, taken together, suggest that the BHE *in vivo* is mediated by a widespread inhibition of inspiratory neurones by E-Dec neurones (Hayashi *et al.* 1996).

Respiratory-modulated rhythmogenic networks functional *in vitro* are postulated to constitute the kernel of the larger network active *in vivo* (Feldman *et al.* 1990), localized in the preBötzinger Complex (preBötC) just caudal and ventral to the compact division of the rostral nucleus ambiguus (Smith *et al.* 1991). Inspiratory neurones predominate in this region, and can be classified based on: (i) the presence of delayed excitation (Type 1 neurones) or sag-rebound (Type 2 neurones) properties in the transverse slice (Rekling *et al.* 1996); and (ii) peri-inspiratory activity, such as Type III inspiratory (hyperpolarized before and after, but active during inspiration) and preinspiratory (active before and after, but hyperpolarized during inspiration; Pre-I) neurones in the *en bloc* preparation (Onimaru & Homma, 1992).

Type 1 and Pre-I neurones are proposed to play a causal role in respiratory rhythmogenesis (Rekling *et al.* 1996; Rekling & Feldman, 1998; Onimaru *et al.* 1988, 1997). We recorded from them, as well as other respiratory neurone types. If the BHE occurred exclusively via inhibition of rhythmogenic neurones, we predicted that only a subset of respiratory neurones would be hyperpolarized during the BHE, and that BHE-lengthened cycles would not be integer multiples of the control period. Instead, if the BHE occurred exclusively by disruption of respiratory drive but not of rhythmogenic mechanisms, we predicted that periods of cycles in which the BHE-lengthened cycles would be integer multiples of the control period, as seen when respiratory drive, but not rhythmogenic networks, are disrupted (Mellen *et al.* 2003). Preliminary results have appeared in abstract form (Mellen & Feldman, 1999).

Methods

Dissection

Sprague–Dawley rats (0–3 days old; $n = 58$) were used. In accordance with methods approved by the Institutional Animal Care and Use Committee, UCLA, rat pups were cooled to 5°C, decerebrated immediately rostral to the superior colliculus and transferred to a bath continuously perfused with artificial cerebrospinal fluid (ACSF) containing (mM): 128.0 NaCl, 3.0 KCl, 1.5 $CaCl_2$, 1.0 $MgSO_4$, 21.0 $NaHCO_3$, 0.5 NaH_2PO_4 and 30.0 glucose, equilibrated with 95% O_2–5% CO_2, at 5°C.

The neuraxis with the heart, oesophagus, carotid artery, trachea, right vagus nerve, and lungs were retained as follows: after exposing the dorsal surface of the neuraxis, the animal was pinned out ventral surface upwards; the sternohyoid and sternomastoid muscles were cut to expose the trachea, vagi and carotid arteries. Musculature underneath and lateral to the right vagus nerve was removed (cleidomastoid, clavotrapezius and ornohyoid muscles). The trachea was cut at the larynx and separated from the oesophagus beneath it. Without damaging the carotid artery or the vagus nerve, the digastric and masseter muscles were removed to expose the ventral surface of the skull, and arteries rostral to the tympanic bulla were cut. The skull was transected rostral to the tympanic bulla, and the left vagus and carotid artery were cut. The occipital bone was removed to expose the ventral surface of the brainstem, and what remained of the skull was removed from the left side. The thorax was then split, and the lungs, heart, oesophagus and trachea were freed. The spinal column was then removed and the spinal cord was transected at the third thoracic segment.

The brainstem was pinned out ventral surface upwards on a Sylgard™ platform, and the lungs stabilized by pinning down the oesophagus at the rostral and caudal ends. After removing the dura from the ventral surface,

the medulla was transected just rostral to the vagus nerve, which corresponded to a transection through the facial nucleus. A saline-filled cannula (22 gauge) connected to a computer-controlled precision syringe pump (Carnegie Medecin M100), with a branch to a manometer, was inserted into the trachea approximately 2 mm caudal to the larynx, and held in place with a suture (Fig. 1). The bath was warmed to 26–28°C before recording activity. The dissection, from start to finish, was routinely completed in under an hour.

Because respiratory efforts persisted following decerebration, the lungs were filled with ACSF so that they did not collapse following opening of the thorax. As a result, we were able to obtain the BHE from the outset with pressure changes in the physiological range (2–3 cmH_2O). In cases in which expiratory lengthening did not occur, we gradually increased lung volume by withdrawing slightly less ACSF from the lungs than was injected. Once expiratory lengthening was observed, lung inflation and deflation were made symmetric.

Recording methods

Ventral root recordings. Inspiratory activity was recorded from ventral roots C1–C3 using a saline-filled low resistance glass suction electrode (100 kΩ). Signals were amplified 15 000–30 000 times, and bandpass filtered (0.3–3 kHz) using Grass P5 differential amplifiers (Grass Instruments, Quincy, MA, USA).

Intracellular recordings. Intracellular current-clamp recordings were carried out using the blind whole-cell patch clamp technique (Blanton *et al.* 1989) from inspiratory and expiratory neurones in a region extending rostrocaudally from the rostral ventral respiratory group to the Bötzinger complex (Smith *et al.* 1991), to depths of 200–600 μm from the ventral surface, near the base of the hypoglossal rootlets. Electrodes were pulled from filamented glass capillary tubing (1.5 mm o.d., 0.86 mm i.d.; A-M Systems). Lucifer Yellow CH (0.2%, Molecular Probes) and biocytin (0.2%, Molecular Probes) were added to the intracellular solution for subsequent identification of recording locations. In order to mitigate sampling bias towards larger cells, electrodes with resistances ranging from 4 to 12 MΩ were used.

Recordings were carried out in current-clamp bridge mode using the Axoclamp-2A amplifier (Axon Instruments). Because of the high input resistance, a 0.01X gain headstage was used. Capacitance was neutralized. An increase in the voltage deflection associated with a high-frequency (100 Hz, 0.2 duty cycle) 120 pA square wave passed through the electrode indicated contact with the ventral surface of the brainstem. The electrode was then quickly advanced 200–500 μm while applying strong positive pressure. Thereafter, the electrode was advanced in 3–5 μm steps, while applying moderate positive pressure and passing 120 pA pulses through the tip. A sudden increase in voltage deflection indicated the close proximity of a cell. Pulse amplitude was then decreased to 20 pA. To facilitate membrane rupture, a hyperpolarizing bias current was passed to hold the electrode at –90 mV. When less than 10 pA of current was required to maintain −90 mV, the membrane was ruptured by applying negative pressure to the electrode tip. Access resistance was 10–20 MΩ. Only neurones with $V_m < -40$ mV and action potential overshoot were studied. Series resistance was balanced before applying bias currents. Input resistance (R_{in}) was estimated by measuring the voltage deflection associated with a 2 s 20 pA hyperpolarizing pulse, applied in mid-expiration. Liquid junction potentials were not compensated. Step currents were applied using

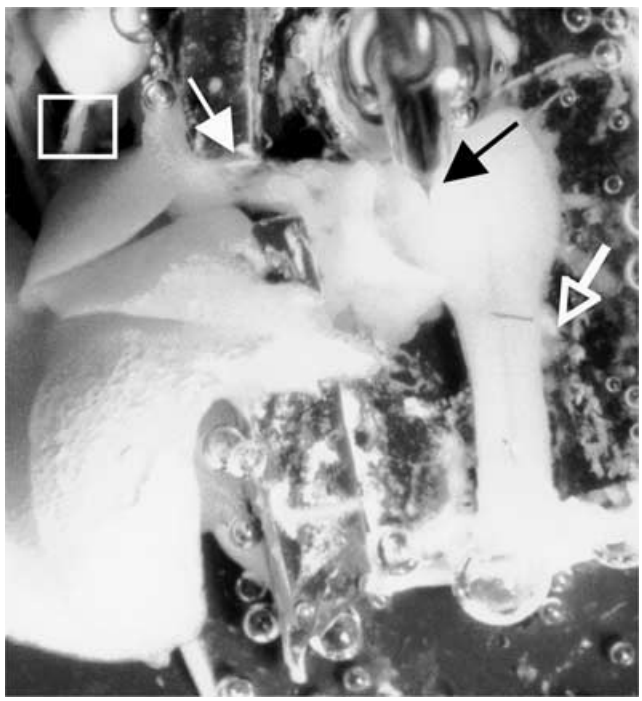

Figure 1. View of the preparation in the recording chamber
The brainstem–spinal cord preparation is pinned out on a Sylgard™ (Dow Corning) platform. An intracellular recording electrode (black arrow) is positioned for recording in the rostral ventrolateral medulla. Population activity is recorded off ventral roots C1–C3 (white hollow arrow). The lungs and the right vagus nerve (thin white arrow) are visible on the right. Pressure changes to the lungs are applied via a cannula inserted in the trachea (white box, upper left).

a pulse generator (AMPI Master 8), triggered by the instrumentation control computer (see below).

Bath application of drugs

In some experiments, pharmacological manipulations were carried out by adding a concentrated agonist–antagonist solution to the ACSF to obtain the appropriate bath concentration. The following pharmacological agents were used (μM): 10 glycine receptor antagonist strychnine (STR), 10 $GABA_A$ antagonist bicuculline (BIC), 20 non-NMDA ionotropic glutamate receptor antagonist 6-cyano-7-nitroquinoxaline-2,3-dione (CNQX), and 10 NMDA receptor antagonist (±)-2-amino-5-phosphonopentanoic acid (APV). Bath application of each drug was followed by an equilibration period of at least 5 min.

Data acquisition, signal processing and instrumentation control

Ventral root recordings, intracellular voltage recordings, applied bias currents and square pulses used to control the syringe pump and pulse generator were digitized at 20 kHz using an A/D–D/A board (AT-MIO-64-E3; National Instruments, Austin, TX, USA) running on a Pentium-based computer under a Windows operating system. These data were displayed using virtual instrumentation developed in LabView™ (National Instruments) and written to hard disk. In addition, time stamps associated with inspiratory onsets and lung inflation and deflation were written to hard disk.

A second computer, equipped with an A/D–D/A board (AT-MIO-16E-10; National Instruments) was used for instrumentation control. Lung inflation and current pulse application were triggered off inspiration with a 3–5 s delay, so that all stimuli were applied before mid-expiration.

Experimental protocol

Lung inflation protocols. Lungs were inflated to volumes of 0.2–0.4 ml at ~0.1 ml s^{-1}, which resulted in steady-state changes of 2–5 mmH_2O within the physiological range (4–7 mmH_2O; Widdicombe, 1961) as measured using a manometer connected to the cannula. Lungs were held inflated until the subsequent inspiratory burst. Inflation protocols were carried out in bouts. Within each bout, lung inflation was repeated three to five times, and cycles with inflation were separated by at least five respiratory cycles in which no inflation was applied. In order to calculate the reversal potential of inflation-induced hyperpolarization in individual neurones, depolarizing and hyperpolarizing bias currents were applied before lung inflation.

Measurement of membrane properties. Delayed excitation, consistent with the presence of transient outward currents (I_A; Connor & Stevens, 1971), and sag rebound response consistent with an h-type current (I_h; Pape *et al.* 1989), were assessed. These step de- and hyperpolarizations were applied 2–4 s after inspiratory onset, i.e. in mid-expiration, so that membrane responses would not be obscured by de- or hyperpolarizing inspiratory drive currents. For expiratory neurones a small hyperpolarizing bias was applied (<30 pA), just sufficient to block impulse activity.

To test for I_A, a hyperpolarizing bias current sufficient to bring the membrane potential below −80 mV was applied, the bridge was balanced, and a depolarizing step current was applied sufficient to elicit tonic impulse activity. To test for I_h, a series of step hyperpolarizations were applied from the resting membrane potential. In addition, this protocol tested for the presence of low-voltage-activated Ca^{2+} conductances.

Data analysis

Motor output analysis. For both control and test cycles within a bout, the cycle period was defined as the interval from one inspiratory burst onset to the next. Within each bout, mean control ($n > 20$) and test ($n > 7$) cycle periods were calculated. Inflation-induced expiratory lengthening was tested using Student's paired t test on experiment means within Origin (Microcal™). The *modulo* function within Excel (Microsoft) was used to test whether test cycle periods were integer multiples of the mean control period within each bout.

Single neurone analysis. Neurones were classified based on their conductances (see Measurement of membrane properties, above) and their membrane trajectories in relation to the respiratory motor pattern (see Introduction). This was done by burst-triggered averaging, i.e. averaging single neurone activity in a 1.5 s peri-inspiratory window, centred on ventral root inspiratory onset. In order to identify how intrinsic properties and synaptic inputs shaped the baseline activity pattern of respiratory neurones, three criteria were used: (i) membrane properties using methods described above; (i) voltage trajectory in control respiratory cycles; and (iii) voltage trajectory in test cycles.

Histology

At the end of each experiment, the brainstem was fixed in 10% formalin for at least 24 h, then sectioned

(200 μm thick) with a Vibratome. Sections were first viewed under fluorescence to locate the Lucifer Yellow-labelled somata. The section containing the soma, as well as three or four neighbouring sections (for a total of 800–1000 μm), were then processed using an avidin–biotin immunoperoxidase kit (Vectastain Elite ABC Kit, Vector Laboratories, Burlingame, CA, USA), mounted on slides, counterstained with Neutral Red and coverslipped in mounting medium (Cytoseal 60, Stephens Scientific). Soma locations were then compiled using a reference set of drawings made from scanned serial sections of a brainstem and a standard neonate rat brain atlas (Altman & Bayer, 1995). Soma locations in relation to the mediolateral and dorsoventral axes were identified based on the relative distance of the soma with respect to the compact formation of the nucleus ambiguus, the inferior olive and the ventral surface; the rostrocaudal locations were estimated based on the number of sections away from the rostral margin of the inferior olive, which in the angle of sectioning used here, was caudal to the facial nucleus. We display our data with reference to the obex, which we define as the point where the central canal opens. Because of tissue damage during sectioning, not all neurones recorded from were included for analysis.

Results

Respiratory motor output response to lung inflation

The mean control respiratory cycle period across experiments ($n = 58$) was 9.5 ± 0.5 s and was stable within each experiment (Fig. 2*A*). Mid-expiratory lung inflation consistently lengthened the test cycle period (Fig. 2*B* and *C* 20.0 ± 1.3 s, $P < 0.01$). While the mean of test cycle period means was a near-integer multiple of the control period, the individual test cycles were widely dispersed (Fig. 2*C*).

Anatomical location of recorded neurones

Neurones ($n = 67$) for which anatomical location could be determined were recorded in and around the preBötC (Fig. 3, right). Neurones were classified as biphasic ($n = 10$), expiratory ($n = 9$), inspiratory ($n = 36$) and pre-inspiratory ($n = 11$). Inspiratory neurones were further classified into subgroups (see Methods). While most inspiratory neurones were clustered at the obex or 240 μm rostral to it, other neurone types were dispersed along the ventral respiratory column (Fig. 3, left).

Biphasic neurones. Biphasic neurones ($n = 10$) were silent in control cycles (Fig. 4*Ai*, top), and fired during expiration when depolarized (Fig. 4*Ai*, bottom). The burst-triggered average revealed a mixture of excitatory and inhibitory drive during inspiration (Fig. 4*Aii*, top). These neurones showed a sag-rebound response to step hyperpolarization (5/9; Fig. 4*Aii*, bottom). The average membrane potential during the

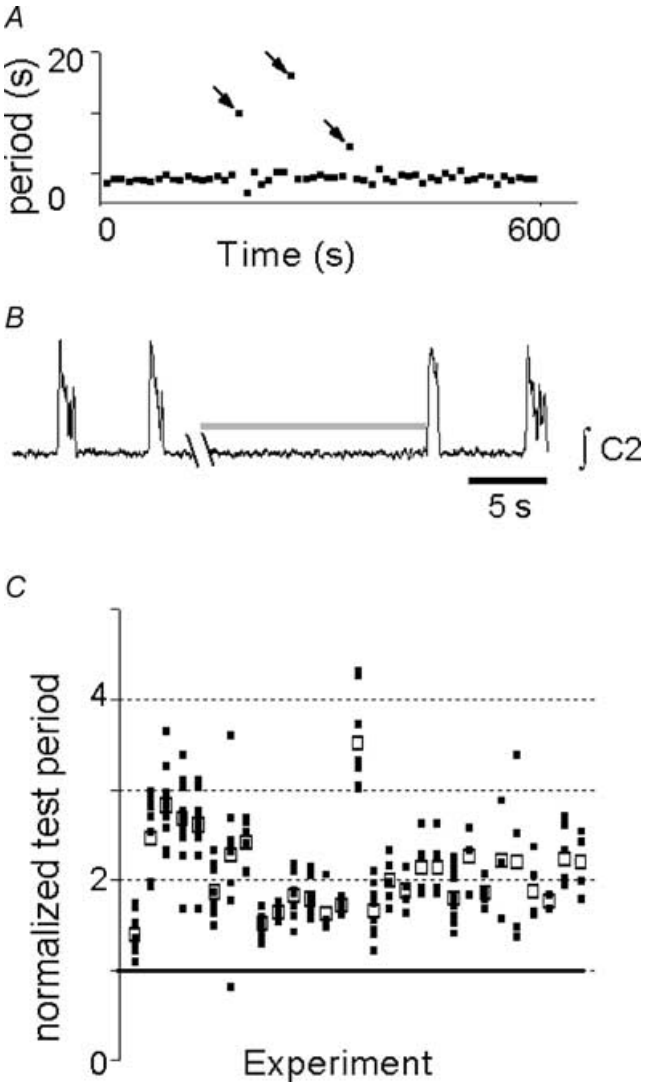

Figure 2. Mid-expiratory inflation lengthened expiration
A, raster plot of periods collected over 10 min. Cycles with inflation (i.e. test cycles) are indicated by arrows. *B*, rectified integrated C2 ventral root activity ($\int$C2) showing typical response to inflation (shaded bar). Syringe pump noise during inflation has been removed for clarity. *C*, test periods, normalized so that control period = 1 (thick continuous line); □, individual normalized test cycle periods; ■, mean test cycle period for each experiment. If expiratory lengthening were due only to suppression of inspiratory drive to motoneurones, then normalized periods would cluster at integer values. While normalized test period means tended to cluster at 2, the individual normalized test period means were dispersed, suggesting that inflation-induced expiratory lengthening is at least in part due to resetting of rhythmogenic networks.

expiratory period of control cycles was −53.7 ± 1.9 mV, with a mean input resistance of 762 ± 153 MΩ. All these neurones were excited during the BHE, and fired briskly during and after inflation (Fig. 4*Bi*, top); the maximal firing rate was 11.8 ± 3.7 Hz. When hyperpolarized below spike threshold, strong inflation-induced depolarizing currents were apparent (Fig. 4*Bi*, bottom). After BIC was applied to block the BHE, these neurones continued to be strongly depolarized during inflation (Fig. 4*Bii*).

Expiratory neurones

Expiratory neurones ($n = 9$) were hyperpolarized during inspiratory bursts, and otherwise fired late in (Fig. 5*A*), or throughout (Fig. 5*B*), expiration at 3.9 ± 2.0 Hz. Membrane potential during expiration was −45.0 ± 5.7 mV, with a mean input resistance of 896 ± 345 MΩ. The BHE-induced hyperpolarization ($n = 3$; Fig. 5*Ai*, bottom), cessation of spiking ($n = 4$; Fig. 5*B*, bottom), or no change from baseline ($n = 2$; not shown). In neurones hyperpolarized during inflation, the reversal potential of the inflation-induced hyperpolarization was −65.0 ± 4.1 mV, more negative than the reversal potential of inspiratory inhibition (− 59.0 ± 4.5 mV, $P < 0.05$; Fig. 5*Aii*).

Inspiratory neurones

Type-1 inspiratory neurones ($n = 12$; Rekling *et al.* 1996) are characterized by ramp-like depolarization during expiration (Fig. 6*Ai*), early onset of inspiratory depolarization (280 ± 44 ms before inspiratory burst onset; Fig. 6*Aii*), and delayed excitation consistent with an I_A-like current (Fig. 6*Aiii*). They were strongly hyperpolarized during the BHE (Fig. 6*Bi*). Applied bias currents (Fig. 6*Bii*, left) amplified or reversed BHE-induced hyperpolarization (ΔV; Fig. 6*Bii*, left), allowing estimation of its reversal potential (V_{rev}; −66.0 ± 3.5 mV ; $n = 9$; Fig. 6*Bii*, right). The average membrane potential of these neurones was −53.0 ± 1.0 mV, with a mean input resistance of 616 ± 100 MΩ. Disruption of fast synaptic transmission by

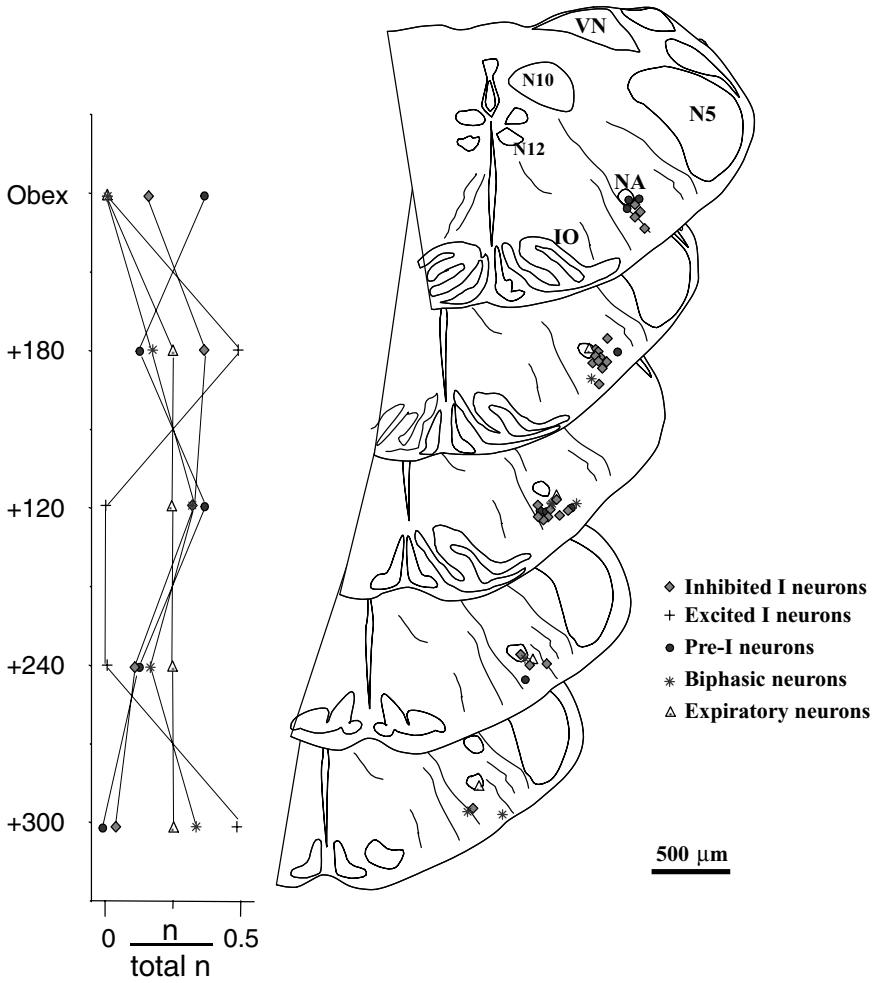

Figure 3. Location of recorded cell somata
Sections are 60 μm apart, with the most caudal segment (top) at the level of the obex. Diamonds, hyperpolarized inspiratory neurones; crosses, excited inspiratory neurones; circles, Pre-I neurones; asterisks, biphasic neurones, hypothesized to correspond to decrementing expiratory neurones *in vivo*; triangles, hyperpolarized expiratory neurones. Abbreviations: CN, cuneate nucleus; N12, hypoglossal nucleus; IO, inferior olive; VN, vestibular nucleus; N5, trigeminal nucleus; N10, dorsal motor nucleus of vagus; NA, nucleus ambiguus. Graph on the left shows normalized cell counts at each section level.

bath application of BIC, STR, CNQX and APV revealed endogenous bursting properties in 3/12 neurones (not shown).

Type III inspiratory neurones (Onimaru *et al.* 1997; $n = 8$) are characterized by pre- and postinspiratory

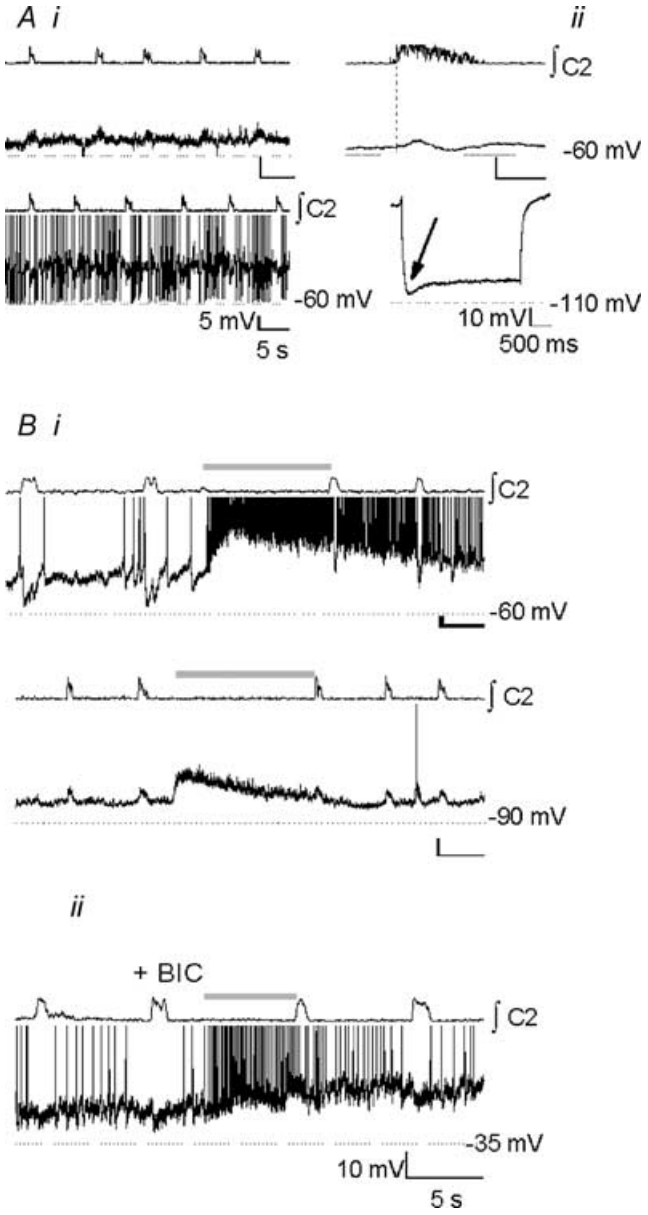

Figure 4. Biphasic neurones
Ai, baseline activity at resting membrane potential (top) and with depolarizing bias to −47 mV (bottom) reveals inhibition during inspiration. *Aii*, top, burst-triggered average activity reveals biphasic activation ($n = 8$ control cycles); bottom, sag-rebound response consistent with an I_h-like current (arrow) was elicited by step hyperpolarization to −100 mV. *Bi*, top, neurones fired briskly with little adaptation during inflation (shaded bar); bottom, inflation-induced depolarization persisted when the neurone was hyperpolarized below spiking threshold. *Bii*, in the presence of BIC (10 μM), the BHE was blocked, but excitatory drive to biphasic neurones was not.

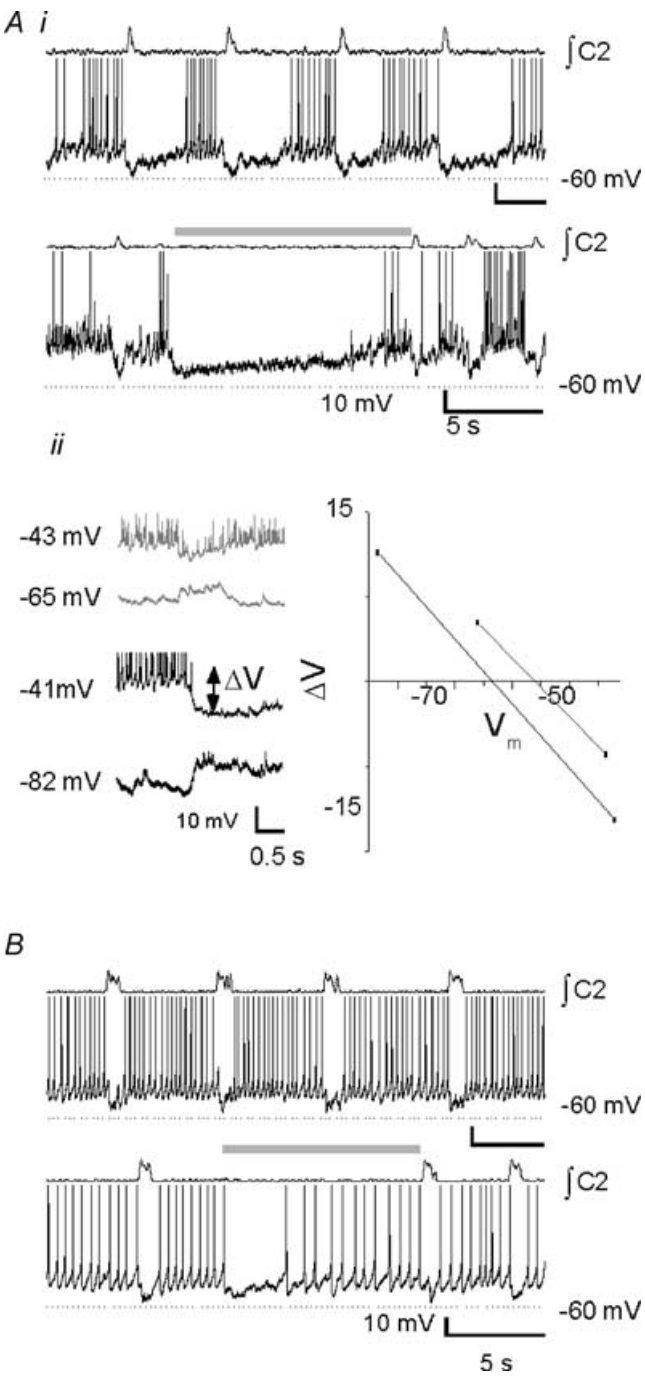

Figure 5. Expiratory neurones
Ai, control activity (top), and inflation-induced inhibition (bottom, shaded bar). *Aii*, left, de- and hyperpolarizing bias currents during inspiratory inhibition (shaded traces) and inflation-induced inhibition (black traces) were applied. Based on the resulting change in membrane potential accompanying inhibitory drive (ΔV) the reversal potential (V_{rev}) for both can be calculated; right: V_{rev} of BHE inhibition was more negative than V_{rev} of inspiratory inhibition. *B*, other expiratory neurones with uniform firing frequency under baseline conditions (top) showed reduced spike frequency during BHE, but little hyperpolarization (bottom).

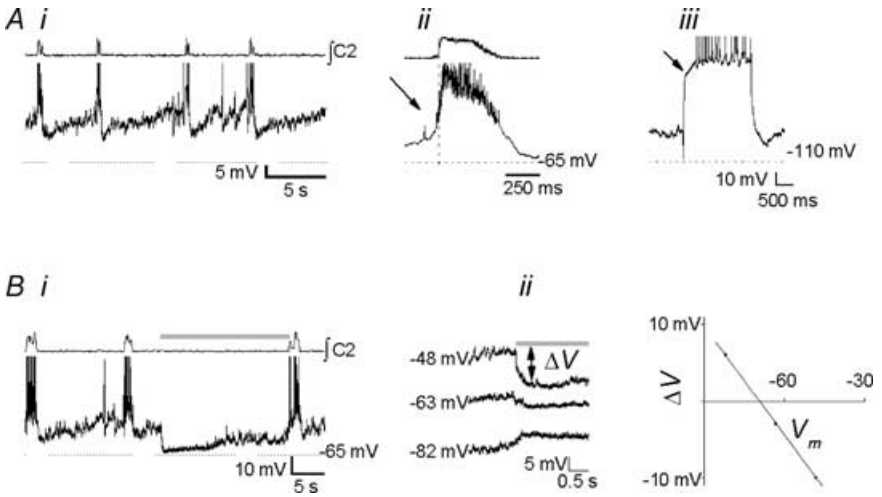

Figure 6. Type-1 inspiratory neurones (Rekling *et al.* 1996)
Ai, control activity. *Aii*, burst-triggered average activity ($n = 8$ control cycles); note preinspiratory depolarization (arrow). *Aiii*, delayed excitation consistent with an I_A-like current (arrow) was elicited by step depolarization to −30 mV from −85 mV. *Bi*, these neurones were strongly hyperpolarized during mid-expiratory inflation (shaded bar). *Bii*, by applying bias currents, inflation-induced hyperpolarization (shaded bar) could be reversed. ΔV, difference between holding membrane potential and membrane potential during inflation (double-headed arrow). The reversal potential (i.e. $\Delta V = 0$) was calculated to be −66 mV.

hyperpolarization (Fig. 7*Ai* and *Aii*); under our experimental conditions, postsynaptic hyperpolarization was typically only apparent when depolarizing bias currents were applied (not shown). They displayed delayed excitation consistent with an I_A-like current (Fig. 7*Aiii*), and were hyperpolarized by inflation (Fig. 7*Bi*). STR did not block hyperpolarization (10 μM, $n = 2$), but did abolish peri-inspiratory hyperpolarization (Fig. 7*Bii*). These neurones had an average membrane potential of −56.0 ± 2.0 mV and a mean input resistance of 553 ± 105 MΩ.

Type 2 neurones ($n = 14$) are characterized by flat membrane trajectory during expiration (Fig. 8*Ai*), depolarization onset coincident with inspiratory onset (Fig. 8*Aii*), and sag-rebound responses to hyperpolarizing current pulses consistent with an I_h current (Fig. 8*Aiii*; Rekling *et al.* 1996). These neurones were weakly hyperpolarized during the BHE (Fig. 8*Bi*). The poor linear fit to ΔV values obtained by applying bias currents during the BHE (Fig. 8*Bii*) may be due to activation of I_h currents at $V_m < -70$ mV, which would shunt the reversed inflation-induced current. Thus, the estimated V_{rev} of the inflation-induced hyperpolarization (−62.5 ± 0.7 mV; $n = 4$; Fig. 8*Bii*, left) is probably too negative. These neurones had an average membrane potential of −56.0 ± 3.0 mV and a mean input resistance of 574 ± 89 MΩ.

Two inspiratory neurones with control activity similar to Type III inspiratory neurones (Fig. 9*Ai*) showed preinspiratory hyperpolarization (Fig. 9*Aii*), and displayed both I_A-like (Fig. 9*Bi*), and I_h-like (Fig. 9*Bii*) properties. They were strongly excited during the BHE (Fig. 9*C*), attaining maximal firing rates of 13.5 ± 3.2 Hz; because of this BHE response they need to be classified separately from hyperpolarized Type III neurones. These neurones had an average membrane potential of −58.0 ± 2.8 mV and a mean input resistance of 750 ± 70 MΩ.

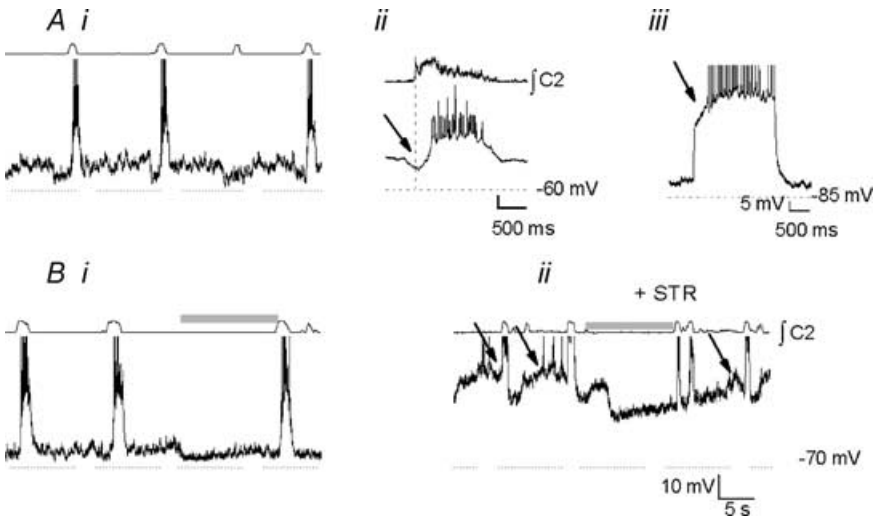

Figure 7. Type-III inspiratory neurones (Onimaru *et al.* 1997)
Ai, baseline activity. Note signature pre- and postinspiratory hyperpolarization, particularly apparent in the cycle in which the neurone failed to fire. *Aii*, burst-triggered average activity ($n = 8$ control cycles). Note preinspiratory inhibition (arrow). *Aiii*, delayed excitation consistent with an I_A-like current (arrow) was elicited by step depolarization to −30 mV from −79 mV. *Bi*, neurones were hyperpolarized by mid-expiratory inflation (shaded bar). *Bii*, following bath application of STR (10 μM), preinspiratory inhibition was blocked (arrows), unmasking the expiratory ramp, the BHE was unaffected, and inflation-induced hyperpolarization persisted.

Pre-I neurones

Pre-I neurones ($n = 11$) fire before and after, and are inhibited during inspiration (Onimaru *et al.* 1988; Fig. 10*A*. Pre-inspiratory firing lasted 690 ± 10 ms and postinspiratory firing lasted 2480 ± 230 ms; inspiratory hyperpolarization began 237 ± 60 ms after inspiratory onset and ended 232 ± 70 ms after inspiratory offset. In cycles in which the inspiratory burst was not accompanied by inhibition of Pre-I neurones, peri-inspiratory excitatory drive was apparent (Fig. 10*A*, arrow). Because strong synaptic drives were present throughout the respiratory cycle, it was impossible to test for I_h or I_A. The response to the BHE was variable. Of 11 neurones recorded, one was immediately excited (Fig. 10*Bi*), four were depolarized within 1 s (680 ± 10 ms; Fig. 10*Bii*) and six were depolarized more than 1 s after inflation (2450 ± 930 ms; Fig. 10*Biii*). Inflation-induced depolarization was blocked following addition of BIC (10 μM; $n = 3$, Fig. 10*C*). These neurones had an average membrane potential of −48.0 ± 1.0 mV and a mean input resistance of 460 ± 100 MΩ. Following disruption of fast synaptic transmission using STR (10 μM), BIC (10 μM), CNQX (20 μM) and APV (20 μM), 2/11 Pre-I neurones exhibited endogenous bursting properties.

Discussion

Significance of systems level responses

In an *en bloc in vitro* preparation with the lungs attached and innervated, we were able to reproduce the BHE. Appropriate expiratory lengthening followed lung inflations at pressures in the physiological range, in contrast to the minutes-long apnoeas obtained in response to lung hyperinflation (Murakoshi & Otsuka, 1985). Neurones were excited or hyperpolarized by inflation, similar to changes accompanying lung inflation but not electrical stimulation of the vagus nerve *in vivo* (Hayashi *et al.* 1996). This suggests that SAR afferents, which underlie the BHE *in vivo* (Adrian, 1933), were selectively activated. The effect of inflation on respiratory frequency and on respiratory-modulated neurones was enhanced compared to responses in the anaesthetized adult rat (Hayashi *et al.* 1996) or cat (Feldman & Cohen, 1978) *in vivo*. This difference may be due to stronger mechanoreceptor activation in fluid-filled (and hence more compliant) lungs, greater sensitivity to pulmonary mechanoreceptor feedback in neonates (Fedorko *et al.* 1988), or anaesthesia-induced neuronal depression in adult *in vivo* preparations (Stucke *et al.*

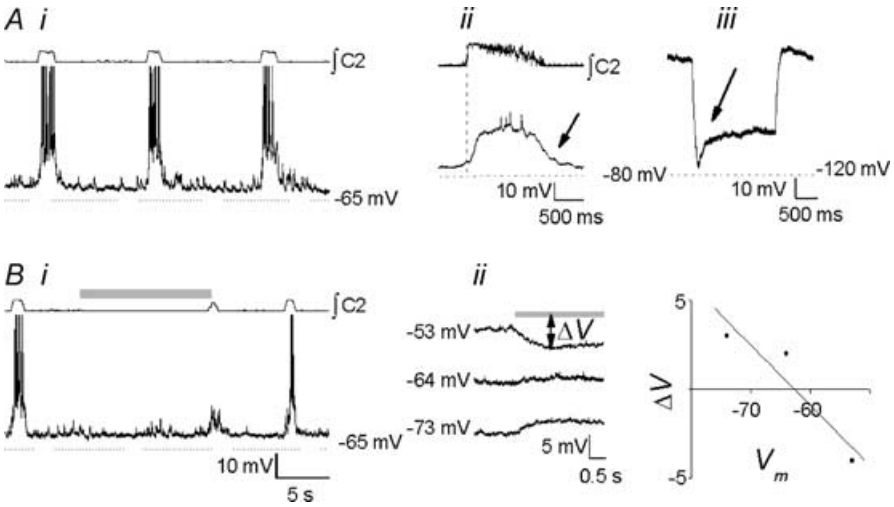

Figure 8. Type 2 neurones (Rekling *et al.* 1996)
Ai, baseline activity. Note flat membrane trajectory during expiration. *Aii*, burst-triggered average activity ($n = 8$ control cycles). Note postinspiratory depolarization (arrow). *Aiii*, sag-rebound response consistent with an I_h-like current was obtained by application of step hyperpolarization to −115 mV from resting mid-expiratory membrane potential (arrow). *Bi*, inflation (shaded bar) produced weak inhibition, but subthreshold inspiratory drive during the first inspiratory burst following inflation offset (arrow). *Bii*, by applying de- and hyperpolarizing bias currents during BHE (shaded bar), inflation-induced inhibition was reversed. ΔV, difference between holding membrane potential and membrane potential during inflation (double-headed arrow). The reversal potential was calculated to be −62.5 mV . This value was probably skewed towards more hyperpolarized values by the shunt associated with the I_h-like current.

2002). Furthermore, the consistent and robust expiratory lengthening obtained here validates the *in vitro* preparation as a model for eupnoeic breathing, as SAR afferent modulation of respiratory rhythm, proposed as the defining criterion of eupnoea (Pluta & Romaniuk, 1990), is not observed during hypoxia-induced gasping *in vivo* (Remmers, 1999; Richter, 2003).

Since our *en bloc* preparation does not include the pons, our results show that medullary networks alone are sufficient to obtain the BHE. Similarly, the BHI is not under control of the pons (Karius *et al.* 1991; Bianchi *et al.* 1995; Mellen & Feldman, 2001), and BH reflexes can be induced following depression of the pons (Feldman *et al.* 1992).

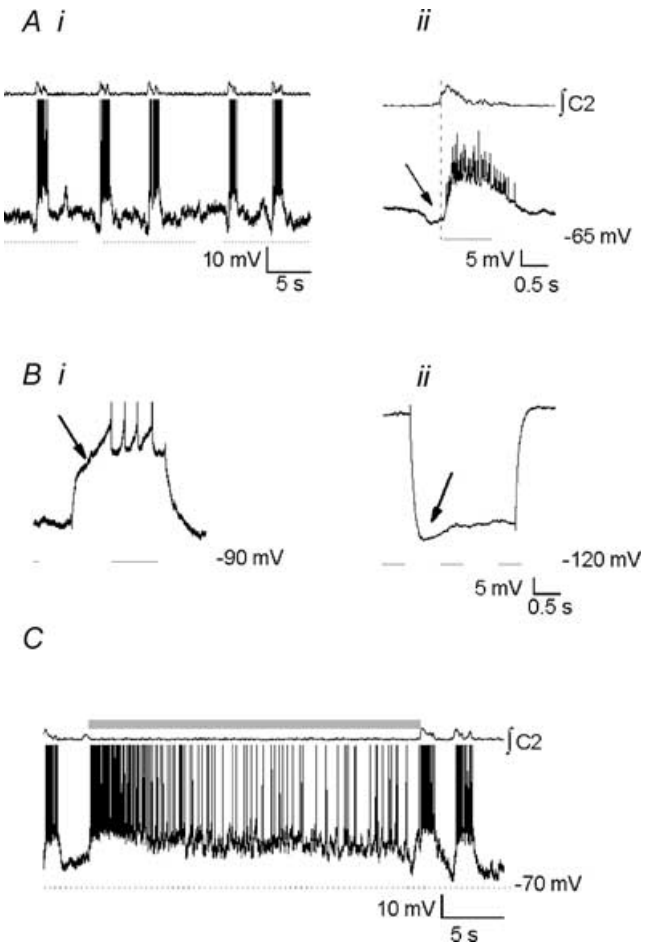

Figure 9. Inspiratory neurones excited by inflation
Ai, baseline activity. *Aii*, burst-triggered baseline average activity ($n = 8$ control cycles); reveals preinspiratory inhibition (arrow) similar to type III neurones. *Bi*, delayed excitation consistent with an I_A-like current (arrow) was elicited by step depolarization to −30 mV from −80 mV . *Bii*, sag-rebound response consistent with an I_h-like current was obtained by application of step hyperpolarization to −110 mV from resting mid-expiratory membrane potential (arrow). *C*, neurones fired briskly during inflation (shaded bar).

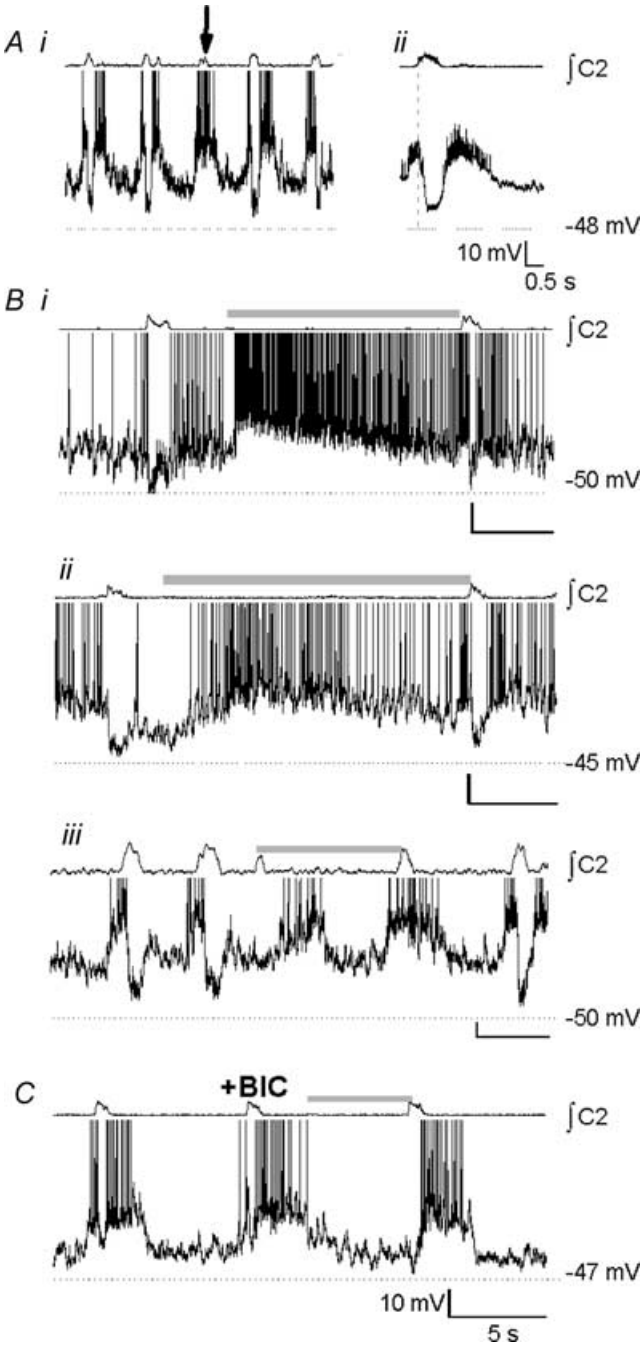

Figure 10. Pre-inspiratory neurones
Ai, baseline activity. Note peri-inspiratory firing in cycle lacking inspiratory inhibition (arrow). *Aii*, burst-triggered average activity. Neurones were depolarized before and after, and hyperpolarized during inspiration. Inspiratory inhibition began 240 ms after inspiratory onset (average of 8 cycles). Both fast (*Bi*) and slow (*Bii* and *iii*) excitation was observed during inflation (shaded bar). *C*, inflation-induced depolarization of Pre-I neurone was blocked by addition of BIC to the perfusate, for a final concentration of 10 μM.

Thus the basic circuitry for the BH reflexes is contained in the medulla, with the pons playing a modulatory role.

We considered the possibility that the BHE bypasses rhythmogenic networks to act exclusively via inhibition of motor output. If this were the case, then test cycle periods would cluster at integer multiples of the control period, as seen when respiratory drive but not rhythm generation is disrupted (Mellen *et al.* 2003). This was not the case, since individual test cycle periods were widely dispersed (Fig. 2*C*). This suggests that the BHE (also) affects rhythmogenic networks.

Anatomical distribution of recorded neurones

Our recording locations spanned the ventral respiratory column (Alheid *et al.* 2002), including regions caudal and rostral to the preBötC that contain premotor networks projecting to cranial and spinal motoneurones. We recorded from Pre-I neurones both rostral to and at the caudal margin of the preBötC. Pre-I neurones at or caudal to the preBötC are bulbospinal abdominal premotoneurones that are driven by more rostral Pre-I neurones (Janczewski *et al.* 2002). Thus, because of the distribution of recording locations, we surmise that our sample includes rhythmogenic and (pre)motor neurones.

One of the goals of this study was to establish whether the BHE could be used to distinguish rhythmogenic from other networks. Because of the heterogeneity of neurones sampled, we are able to evaluate whether this distinction is possible. In the sections that follow, we interpret the responses of expiratory, inspiratory and Pre-I neurones in the context of findings *in vivo* and *in vitro*.

Biphasic neurones

Biphasic neurones showed weak respiratory modulation (Fig. 4*A*), but were strongly excited by lung inflation. The strong depolarizing drive revealed when these neurones were hyperpolarized by current injection (Fig. 4*Bi*, bottom) indicates that lung inflation-induced firing was due to increased synaptic drive. These attributes closely match those of SAR relay neurones in adult rats *in vivo*, which are found in the dorsal medulla (Bonham & McCrimmon, 1990; Ezure *et al.* 2002). Because of their location in the ventral respiratory column, biphasic neurones are likely to be third-order neurones in the pathway mediating the BHE. Based on the time course of inflation-induced hyperpolarization of expiratory (Fig. 5) and inspiratory neurones (Figs 6–8), we hypothesize that biphasic neurones inhibit respiratory neurones involved in generating and relaying respiratory drive.

In adult mammals *in vivo*, two classes of neurones are hypothesized to have the same inhibitory function as we ascribe to biphasic neurones *in vitro*: E-Dec neurones (Hayashi *et al.* 1996), identified as glycinergic (Ezure *et al.* 2003), and Late-I neurones (Cohen *et al.* 1993; Haji *et al.* 2002), inferred to be GABAergic (Haji *et al.* 1999, 2002). The finding that the BHE *in vitro* was unaffected by the glycine receptor antagonist strychnine (Fig. 7) would suggest that biphasic neurones are GABAergic, and thus correspond to Late-I neurones. One caveat is that the transmitter phenotype of biphasic neurones could undergo a developmentally regulated transition from GABA to glycine, as observed elsewhere in the rat CNS (Bruning *et al.* 1990; Colin *et al.* 1998; Turecek & Trussell, 2002; Nabekura *et al.* 2004). Relating biphasic neurones in neonates *in vitro* to adult *in vivo* neurone types is further complicated by the fact that biphasic neurones show weaker respiratory modulation and stronger afferent feedback modulation than either E-Dec or I-Late neurones in adults *in vivo*. The weak respiratory modulation of biphasic neurones could result from the absence in our preparation of the pons, which contains neurones that fire in the postinspiratory phase (Dick *et al.* 1994). The stronger afferent modulation of biphasic neurones may also be due to the absence of anaesthesia-induced increase in GABAergic inhibition (Olsen, 1998; Stucke *et al.* 2002), or their higher input resistance, due to fewer dendritic branches and synaptic inputs in neonatal rat medullary neurones (Hilaire & Duron, 1999).

Expiratory neurones

Most expiratory neurones were hyperpolarized during the BHE. This is consistent with the hypothesis that propriobulbar expiratory neurones provide excitatory drive to rhythmogenic preBötC networks (Smith *et al.* 1993). Alternatively, some of these neurones may have been cranial motoneurones, which are active during expiration and are inhibited by electrical stimulation of the vagus (Hayashi & McCrimmon, 1996). We found that the reversal potential of the BHE-induced hyperpolarization was more negative than that accompanying inspiratory bursts (Fig. 5*Aii*). Inhibition of expiratory neurones during inspiration is glycinergic in neonatal rats (Shao & Feldman, 1997). We hypothesize that hypepolarization necessary for the BHE is GABAergic. This is supported by the observation that the BHE persisted in the presence of strychnine (Fig. 7*Bii*), but was blocked by bicuculline (Figs 4*Bii* and 10*C*). The more negative reversal potential of the BHE-induced inhibition may be due to coactivation of K^+-permeable $GABA_B$ receptor-linked channels in preBötC neurones in the neonatal mouse (Zhang *et al.* 1999).

Inspiratory neurones

Inspiratory neurones were hyperpolarized during the BHE. Type 1 and Type III neurones, which display delayed excitation consistent with I_A but not sag-rebound properties consistent with I_h, were strongly hyperpolarized by lung inflation (Fig. 6*Bi*). For these neurones, their $\Delta V/V$ plots were well fitted by straight lines (Fig. 6*Bii*). Inflation-induced hyperpolarization would partially deinactivate I_A, and so could amplify inflation-induced inhibition by delaying the postinflation return to resting V_m.

By contrast, inflation-induced hyperpolarization was markedly smaller in Type 2 neurones. The reversal potential for BHE-induced hyperpolarization in Type 2 neurones is likely to be less negative than the estimates we obtained; by biasing V_m below −70 mV, inflation-induced hyperpolarization was reversed, but because of partial activation of I_h (Thoby-Brisson *et al.* 2000), it would also be shunted. This may account for the poor linear fit to points in $\Delta V/V_m$ plots that included values at holding potentials at which I_h was weakly, then more strongly activated (Fig. 8*Bii*). While the reversal potential for Cl^--mediated hyperpolarization (~ -75 mV in neonatal rats; Shao & Feldman, 1997) is well below the I_h activation threshold (−55 mV; Thoby-Brisson *et al.* 2000), the sag-rebound characteristic of I_h activation (Fig. 8*Aiii*) is not apparent during inflation-induced hyperpolarization (Fig. 8*Bi* and *Bii*), suggesting that weak hyperpolarizations during the BHE in Type 2 neurones is not due to immediate I_h-induced shunting of inhibitory drive.

A subset of I neurones, qualitatively similar to Type III neurones, were strongly excited during the BHE (Fig. 9). Thus, despite their similar baseline activity pattern, it is unlikely that they are functionally equivalent to Type III neurones hyperpolarized during the BHE. Their strong activation during the BHE suggests that they mediate restoration of expiratory flow.

Type 1 neurones are proposed to play a causal role in respiratory rhythmogenesis (Rekling *et al.* 1996). Respiratory period is hypothesized to be strongly modulated by changes in membrane potential of rhythmogenic neurones (Smith *et al.* 1993). A generic prediction of models of bursting mechanisms is that cycle period varies with rhythmogenic neurone membrane potential; above some threshold, cycle period lengthens as membrane potential hyperpolarizes (ibid.). Thus, the strong hyperpolarization of Type 1 neurones during the BHE is consistent with their hypothesized role as constituents of the respiratory rhythm generator (Rekling *et al.* 1996; Rekling & Feldman, 1998). By the same logic, the weaker hyperpolarization seen in Type 2 neurones suggests that they are not constituents of a voltage-dependent rhythmogenic network, consistent with the conjecture that they are premotoneurones (Rekling *et al.* 1996).

Although the strong hyperpolarization of Type 1 neurones provides a mechanism for the BHE's action on rhythmogenic networks, this evidence is weak. If Type 1 neurones were the only class of inspiratory neurones hyperpolarized by the BHE, then the inference that Type 1 neurones were necessary for respiratory rhythmogenesis would be relatively straightforward. The observation that the majority of inspiratory neurones were hyperpolarized suggests that both rhythmogenic and relay neurones are modulated during the BHE, and strength of hyperpolarization must be interpreted carefully. Thus functional inferences based solely on responses during the BHE are by necessity incomplete. When combined with other criteria, including immunohistochemistry (Gray *et al.* 1999, Stornetta *et al.* 2003) and morphology, responses during the BHE may support stronger functional inferences.

Relating *in vitro* inspiratory neurone classes to those used *in vivo* on the basis of their responses during the BHE is difficult because, while differences in BHE-induced hyperpolarization were apparent in distinct inspiratory neurone classes *in vitro* (Figs 6–8), such differences are not observed across inspiratory neurone classes *in vivo*. This may be due to the developmental changes (Hilaire & Duron, 1999) or experimental differences (Stucke *et al.* 2002) indicated above.

Pre-I neurones

Pre-I neurones are proposed as essential constituents of respiratory rhythm-generating networks (Onimaru & Homma, 1987). Pharmacological manipulations (Mellen *et al.* 2003) and optical recordings (Onimaru & Homma, 2003) suggest that respiratory rhythm is generated by the interaction between preBötC and rostral Pre-I networks, each of which, under appropriate conditions, can determine inspiratory burst timing. The causal role of Pre-I neurones is supported by the consistent observation of Pre-I firing immediately preceding inspiratory burst onset during control cycles. During the BHE, however, that coupling was lost; lung inflation induced either an immediate (Fig. 10*Bi*) or delayed (Fig. 10*Bii* and *Biii*) Pre-I neurone firing, followed not immediately but rather seconds later by the subsequent inspiratory burst onset. Mid-expiratory Pre-I firing during the BHE suggests that in test cycles, Pre-I activity does not determine inspiratory

burst onset. This mid-expiratory activity is probably due to disinhibition rather than excitatory drive from second- or third-order relay neurones, since it is blocked by BIC (Fig. 10*C*). Because caudal Pre-I neurones project bulbospinally to motoneurones innervating expiratory abdominal muscles (Janczewski *et al.* 2002), Pre-I neurone activity during the BHE may underlie an airway-clearing manoeuvre via abdominal muscle contraction. Such a response is seen in dogs, in response to moderate airway pressure changes (Koepchen *et al.* 1973; Bajic *et al.* 1992; reviewed by Iscoe, 1998). Pre-I and biphasic neurones are both hyperpolarized during inspiration and excited during the BHE; thus, these neurones could represent extremes of a continuum. The following observations suggest that this is not the case. In the presence of inflation during inspiration, biphasic neurones fired during inspiration, whereas Pre-I neurones were hyperpolarized during inspiration (Mellen & Feldman, 2001). In addition, bicuculline had no effect on the biphasic neurone response to lung inflation (Fig. 4) but blocked the Pre-I neurone response (Fig. 10). Thus, these neurone classes appear to be distinct. Based on their responses to phasic inflation, Pre-I neurones may correspond to augmenting expiratory neurones *in vivo* (Parkes *et al.* 1994; Hayashi *et al.* 1996).

Mappings between in vitro and in vivo preparations

An early discussion of the relationship between *in vitro* and *in vivo* preparations (Feldman *et al.* 1990) was framed in terms of two alternative hypotheses. In the *reductionist* hypothesis, the basic mechanisms for respiratory rhythm generation were stipulated to be the same *in vivo* at all ages and *in vitro*, so that differences between them were due to removal of nonessential complexity *in vitro*; in the *transformational* hypothesis, mechanisms for respiratory rhythm generation in neonatal rodents *in vitro* and in adult rodents *in vivo* were stipulated to be qualitatively different because of differences in milieu, afferent modulation and development. More recent findings do not support the strong form of either hypothesis. On the one hand, important morphological and electrophysiological changes occur over the course of development (Richter & Spyer, 2001). On the other hand, several key observations driving hypotheses about rhythmogenic mechanisms in neonate *in vitro* rodent preparations are congruent with those in adult rats *in vivo* (Gray *et al.* 2001; Mellen *et al.* 2003), suggesting that despite developmental transformations, neonatal *in vitro* preparations are useful model systems for studying eupnoea in adult mammals *in vivo*.

Despite the differences in adult *in vivo* and neonate *in vitro* respiratory neurone activity during the BHE, changes in activity during the BHE are qualitatively the same: neurones hyperpolarized during inspiration are depolarized during lung inflation, and inspiratory neurones are inhibited. More importantly, the observed differences could be accounted for by developmental or methodological differences proposed by others as factors that need to be taken into account when comparing *in vitro* and *in vivo* data (Richter & Spyer, 2001), suggesting that the transformation of cellular and network properties from *in vitro* to *in vivo* conditions obeys identified mechanisms.

References

Adrian ED (1933). Afferent impulses in the vagus and their effect on respiration. *J Physiol* **79**, 332–358.

Alheid GF, Gray PA, Jiang MC, Feldman JL & McCrimmon DR (2002). Parvalbumin in respiratory neurons of the ventrolateral medulla of the adult rat. *J Neurocytol* **31**, 693–717.

Altman J & Bayer SA (1995). *Atlas of Prenatal Rat Brain Development*. CRC Press, Boca Raton, FL, USA.

Bajic J, Zuperku EJ, Tonkovic-Capin M & Hopp FA (1992). Expiratory bulbospinal neurons of dogs. I. Control of discharge patterns by pulmonary stretch receptors. *Am J Physiol* **262**, R1075–R1086.

Bianchi AL, Denavit-Saubie M & Champagnat J (1995). Central control of breathing in mammals: neuronal circuitry, membrane properties, and neurotransmitters. *Physiol Rev* **75**, 1–45.

Blanton MG, Lo Turco JJ & Kriegstein AR (1989). Whole cell recording from neurons in slices of reptilian and mammalian cerebral cortex. *J Neurosci Meth* **30**, 203–210.

Bonham AC, Coles SK & McCrimmon DR (1993). Pulmonary stretch receptor afferents activate excitatory amino acid receptors in the nucleus tractus solitarii in rats. *J Physiol* **464**, 725–745.

Bonham AC & McCrimmon DR (1990). Neurons in a discrete region of the nucleus tractus solitarius are required for the Breuer-Hering reflex in rat. *J Physiol (Lond)* **427**, 261–280.

Breuer J (1868). Self-steering of respiration through the nervus vagus [English transl.]. In *Breathing: Hering-Breuer Centenary Symposium*. ed. Porter, R, pp. 365–394. Churchill, London (1970).

Bruning G, Bauer R & Baumgarten HG (1990). Postnatal development of [^{3}H]flunitrazepam and [^{3}H]strychnine binding sites in rat spinal cord localized by quantitative autoradiography. *Neurosci Lett* **110** (1–2), 6–10.

Cohen MI, Huang WX, Barnhardt R & See WR (1993). Timing of medullary late-inspiratory neuron discharges: vagal afferent effects indicate possible off-switch function. *J Neurophysiol* **69** (5), 1784–1787.

Colin I, Rostaing P, Augustin A & Triller A (1998). Localization of components of glycinergic synapses during rat spinal cord development. *J Comp Neurol* **398** (3), 359–372.

Connor JA & Stevens CF (1971). Voltage clamp studies of a transient outward membrane current in gastropod neural somata. *J Physiol* **213**, 21–30.

Dick TE, Bellingham MC & Richter DW (1994). Pontine respiratory neurons in anesthetized cats. *Brain Res* **636** (2), 259–269.

Dutschmann M & Paton JF (2003). Whole cell recordings from respiratory neurones in an arterially perfused *in situ* neonatal rat preparation. *Exp Physiol* **88** (6), 725–732.

von Euler C (1983). On the origin and pattern control of breathing rhythmicity in mammals. *Symp Soc Exp Biol* **37**, 469–485.

Ezure K & Manabe M (1988). Decrementing expiratory neurons of the Bötzinger complex. II. Direct inhibitory synaptic linkage with ventral respiratory group neurons. *Exp Brain Res* **72** (1), 159–166.

Ezure K & Tanaka I (1996). Pump neurons of the nucleus of the solitary tract project widely to the medulla. *Neurosci Lett* **215** (2), 123–126.

Ezure K & Tanaka I (2000). Lung inflation inhibits rapidly adapting receptor relay neurons in the rat. *Neuroreport* **11** (8), 1709–1712.

Ezure K, Tanaka I & Kondo M (2003). Glycine is used as a transmitter by decrementing expiratory neurons of the ventrolateral medulla in the rat. *J Neurosci* **23** (26), 8941–8948.

Ezure K, Tanaka I, Saito Y & Otake K (2002). Axonal projections of pulmonary slowly adapting receptor relay neurons in the rat. *J Comp Neurol* **446** (1), 81–94.

Fedorko L, Kelly EN & England SJ (1988). Importance of vagal afferents in determining ventilation in newborn rats. *J App Physiol* **65**, 1033–1039.

Feldman J (1986). Neurophysiology of breathing in mammals. In *Handbook of Physiology; Section I: The Neurons System,* vol. IV. ed. Bloom, F, pp. 463–524. American Physiological Society, Bethesda MD.

Feldman JL & Cohen MI (1978). Relation between expiratory duration and rostral medullary expiratory neuronal discharge. *Brain Res* **141** (1), 172–178.

Feldman JL, Smith JC, Ellenberger HH, Connelly CA, Liu GS, Greer JJ, Lindsay AD & Otto MR (1990). Neurogenesis of respiratory rhythm and pattern: emerging concepts. *Am J Physiol* **259**, R879–R886.

Feldman JL, Windhorst U, Anders K & Richter DW (1992). Synaptic interaction between medullary respiratory neurones during apneusis induced by NMDA-receptor blockade in cat. *J Physiol* **450**, 303–323.

Gray P, Rekling J, Bocchiaro C & Feldman J (1999). Modulation of respiratory frequency by peptidergic input to rhythmogenic neurons in the preBötzinger complex. *Science* **286**, 1566–1568.

Gray PA, Janczewski WA, Mellen N, McCrimmon DR & Feldman JL (2001). Normal breathing requires preBötzinger complex neurokinin-1 receptor-expressing neurons. *Nat Neurosci* **4** (9), 927–930.

Haji A, Okazaki M & Takeda R (1999). GABA (A) receptor-mediated inspiratory termination evoked by vagal stimulation in decerebrate cats. *Neuropharmacology* **38** (9), 1261–1272.

Haji A, Okazaki M, Yamazaki H & Takeda R (2002). Physiological properties of late inspiratory neurons and their possible involvement in inspiratory off-switching in cats. *J Neurophysiol* **87** (2), 1057–1067.

Hayashi F, Coles SK & McCrimmon DR (1996). Respiratory neurons mediating the Breuer-Hering reflex prolongation of expiration in rat. *J Neurosci* **16**, 6526–6536.

Hayashi F & McCrimmon DR (1996). Respiratory motor responses to cranial nerve afferent stimulation in rats. *Am J Physiol* **271**, R1054–R1062.

Hilaire G & Duron B (1999). Maturation of the mammalian respiratory system. *Physiol Rev* **79** (2), 325–360.

Iscoe S (1998). Control of abdominal muscles. *Prog Neurobiol* **56** (4), 433–450.

Janczewski WA, Onimaru H, Homma I & Feldman JL (2002). Opioid-resistant respiratory pathway from the preinspiratory neurones to abdominal muscles: *in vivo* and *in vitro* study in the newborn rat. *J Physiol* **545** (3), 1017–1026.

Karius DR, Ling LM & Speck DF (1991). Lesions of the rostral dorsolateral pons have no effect on afferent-evoked inhibition of inspiration. *Brain Res* **559** (1), 22–28.

Koepchen HP, Klüssendorf D & Philipp U (1973). Mechanisms of central transmission of respiratory reflexes. *Acta Neurobiol Exp* **33**, 287–299.

Lindsey BG, Morris KF, Segers LS & Shannon R (2000). Respiratory neuronal assemblies. *Respir Physiol* **122**, 183–196.

Lindsey BG, Segers LS & Shannon R (1987). Functional associations among simultaneously monitored lateral medullary respiratory neurons in the cat. II. Evidence for inhibitory actions of expiratory neurons. *J Neurophysiol* **57** (4), 1101–1117.

Manabe M & Ezure K (1988). Decrementing expiratory neurons of the Bötzinger complex. I. Response to lung inflation and axonal projection. *Exp Brain Res* **72** (1), 150–158.

Mellen NM & Feldman JL (1997). Vagal stimulation induces expiratory lengthening in the *in vitro* neonate rat. *J App Physiol* **83**, 1607–1611.

Mellen NM & Feldman JL (1999). Functional analysis of respiratory neurons using the Breuer-Hering reflex *in vitro*. *Soc Neurosci Abstract* **24** (1), 532.

Mellen NM & Feldman JL (2000). Phasic lung inflation shortens inspiration and respiratory period in the lung-attached neonate rat brain stem spinal cord. *J Neurophysiol* **83**, 3165–3168.

Mellen NM & Feldman JL (2001). Phasic vagal sensory feedback transforms respiratory neuron activity *in vitro*. *J Neurosci* **21** (18), 7363–7371.

Mellen NM, Janczewski WA, Bocchiaro CM & Feldman JL (2003). Opioid-induced quantal slowing reveals dual networks for respiratory rhythm generation. *Neuron* **37** (5), 821–826.

Mitchell GS & Johnson SM (2003). Neuroplasticity in respiratory motor control. *J Appl Physiol* **94** (1), 358–374.

Murakoshi T & Otsuka M (1985). Respiratory reflexes in an isolated brainstem–lung preparation of the newborn rat: possible involvement of gamma-aminobutyric acid and glycine. *Neurosci Lett* **62**, 63–68.

Nabekura J, Katsurabayashi S, Kakazu Y, Shibata S, Matsubara A, Jinno S, Mizoguchi Y, Sasaki A & Ishibashi H (2004). Developmental switch from GABA to glycine release in single central synaptic terminals. *Nature Nsci* **7** (1), 17–23.

Olsen RW (1998). The molecular mechanism of action of general anesthetics: structural aspects of interactions with GABA (A) receptors. *Toxicol Lett* **100–101**, 193–201.

Onimaru H, Arata A & Homma I (1988). Primary respiratory rhythm generator in the medulla of brainstem–spinal cord preparation from newborn rat. *Brain Res* **445** (2), 314–324.

Onimaru H, Arata A & Homma I (1997). Neuronal mechanisms of respiratory rhythm generation: an approach using *in vitro* preparation. *Jap J Physiol* **47**, 385–403.

Onimaru H & Homma I (1987). Respiratory rhythm generator neurons in medulla of brainstem–spinal cord preparation from newborn rat. *Brain Res* **403**, 380–384.

Onimaru H & Homma I (1992). Whole cell recordings from respiratory neurons in the medulla of brainstem–spinal cord preparations isolated from newborn rats. *Pflügers Arch* **420** (3–4), 399–406.

Onimaru H & Homma I (2003). A novel functional neuron group for respiratory rhythm generation in the ventral medulla. *J Neurosci* **23** (4), 1478–1486.

Pape HC & McCormick DA (1989). Noradrenaline and serotonin selectively modulate thalamic burst firing by enhancing a hyperpolarization-activated cation current. *Nature* **340**, 715–718.

Parkes MJ, Lara-Munoz JP, Izzo PN & Spyer KM (1994). Responses of ventral respiratory neurones in the rat to vagus stimulation and the functional division of expiration. *J Physiol* **476** (1), 131–139.

Pluta R & Romaniuk JR (1990). Recovery of breathing pattern after 15 min of cerebral ischemia in rabbits. *J App Physiol* **69**, 1676–1681.

Rekling JC, Champagnat J & Denavit-Saubié M (1996). Electroresponsive properties and membrane potential trajectories of three types of inspiratory neurons in the newborn mouse brain stem *in vitro*. *J Neurophysiol* **75**, 795–810.

Rekling JC & Feldman JL (1998). PreBötzinger complex and pacemaker neurons: hypothesized site and kernel for respiratory rhythm generation. *Annu Rev Physiol* **60**, 385–405.

Remmers JE (1999). Central neural control of breathing. In *Lung Biology in Health and Disease*: *Control of Breathing in Health and Disease*, ed. Altose M & Kawami, Y, pp. 1–41. M. Dekker, New York, NY.

Richter DW (2003). Commentary on eupneic breathing patterns and gasping. *Respir Physiol Neurobiol* **139** (1), 121–130.

Richter DW & Spyer KM (2001). Studying rhythmogenesis of breathing: comparison of *in vivo* and *in vitro* models. *Trends Neurosci* **24** (8), 464–472.

Schelegle ES & Green JF (2001). An overview of the anatomy and physiology of slowly adapting pulmonary stretch receptors. *Respir Physiol* **125**, 17–31.

Schwarzacher SW, Smith JC & Richter DW (1995). Pre-Bötzinger complex in the cat. *J Neurophysiol* **73** (4), 1452–1461.

Segers LS, Shannon R, Saporta S & Lindsey BG (1987). Functional associations among simultaneously monitored lateral medullary respiratory neurons in the cat. I. Evidence for excitatory and inhibitory actions of inspiratory neurons. *J Neurophysiol* **57** (4), 1078–1100.

Shao XM & Feldman JL (1997). Respiratory rhythm generation and synaptic inhibition of expiratory neurons in pre-Bötzinger complex: differential roles of glycinergic and GABAergic neural transmission. *J Neurophys* **77** (4), 1853–1860.

Smith JC, Ellenberger HH, Ballanyi K, Richter DW & Feldman JL (1991). Pre-Bötzinger complex: a brainstem region that may generate respiratory rhythm in mammals. *Science* **254**, 726–729.

Smith JC & Feldman JL (1987). *In vitro* brainstem–spinal cord preparations for study of motor systems for mammalian respiration and locomotion. *J Neurosci Meth* **21**, 321–333.

Smith JC, Funk G, Johnson S & Feldman JL (1993). Cellular and synaptic mechanisms generating respiratory rhythm: insights from *in vitro* and computational studies. In *Respiratory Control: Central and Peripheral Mechanisms*, ed. Speck DF, Dekin MS, Revelette WR & Frazier, DT, pp. 39–42. The University Press of Kentucky, Lexington KY, USA.

Stornetta RL, Rosin DL, Wang H, Sevigny CP, Weston MC & Guyenet PG (2003). A group of glutamatergic interneurons expressing high levels of both neurokinin-1 receptors and somatostatin identifies the region of the pre-Bötzinger complex. *J Comp Neurol* **455** (4), 499–512.

Stucke AG, Stuth EA, Tonkovic-Capin V, Tonkovic-Capin M, Hopp FA, Kampine JP & Zuperku EJ (2002). Effects of halothane and sevoflurane on inhibitory neurotransmission to medullary expiratory neurons in a decerebrate dog model. *Anesthesiology* **96** (4), 955–962.

Thoby-Brisson M, Telgkamp P & Ramirez J-M (2000). The role of the hyperpolarization-activated current in modulating rhythmic activity in the isolated respiratory network of mice. *J Neurosci* **20** (8), 2994–3005.

Turecek R & Trussell LO (2002). Reciprocal developmental regulation of presynaptic ionotropic receptors. *Proc Natl Acad Sci U S A* **99** (21), 13884–13889.

Widdicombe JG (1961). Respiratory reflexes in man and other mammalian species. *Clin Sci* **21**, 163–170.

Widdicombe J & Lee LY (2001). Airway reflexes, autonomic function, and cardiovascular responses. *Environ Health Perspect* **109** (Suppl. 4), 579–584.

Zhang W, Elsen F, Barnbrock A & Richter DW (1999). Postnatal development of $GABA_B$ receptor-mediated modulation of voltage-activated Ca^{2+} currents in mouse brain-stem neurons. *Eur J Neurosci* **11** (7), 2332–2342.

Acknowledgements

This research was supported by the following grants: The American Lung Association, RG 105-N; and National Institutes of Health, HL40959 and HL37941.